Interaction of a Cumulus Cloud Ensemble with the Large-Scale Environment. Part III: Semi-Prognostic Test of the Arakawa-Schubert Cumulus Parameterization

STEPHEN J. LORD[1]

Department of Atmospheric Sciences, University of California, Los Angeles 90024

(Manuscript received 26 August 1980, in final form 14 September 1981)

ABSTRACT

The verification of the Arakawa and Schubert (1974) cumulus parameterization is continued using a semi-prognostic approach. Observed data from Phase III of GATE are used to provide estimates of the large-scale forcing of a cumulus ensemble at each observation time. Instantaneous values of the precipitation and the warming and drying due to cumulus convection are calculated using the parameterization.

The results show that the calculated precipitation agrees very well with estimates from the observed large-scale moisture budget and from radar observations. The calculated vertical profiles of cumulus warming and drying also are quite similar to the observed. It is shown that the closure assumption adopted in the parameterization (the cloud-work function quasi-equilibrium) results in errors of generally <10% in the calculated precipitation. The sensitivity of the parameterization to some assumptions of the cloud ensemble model and the solution method for the cloud-base mass flux is investigated.

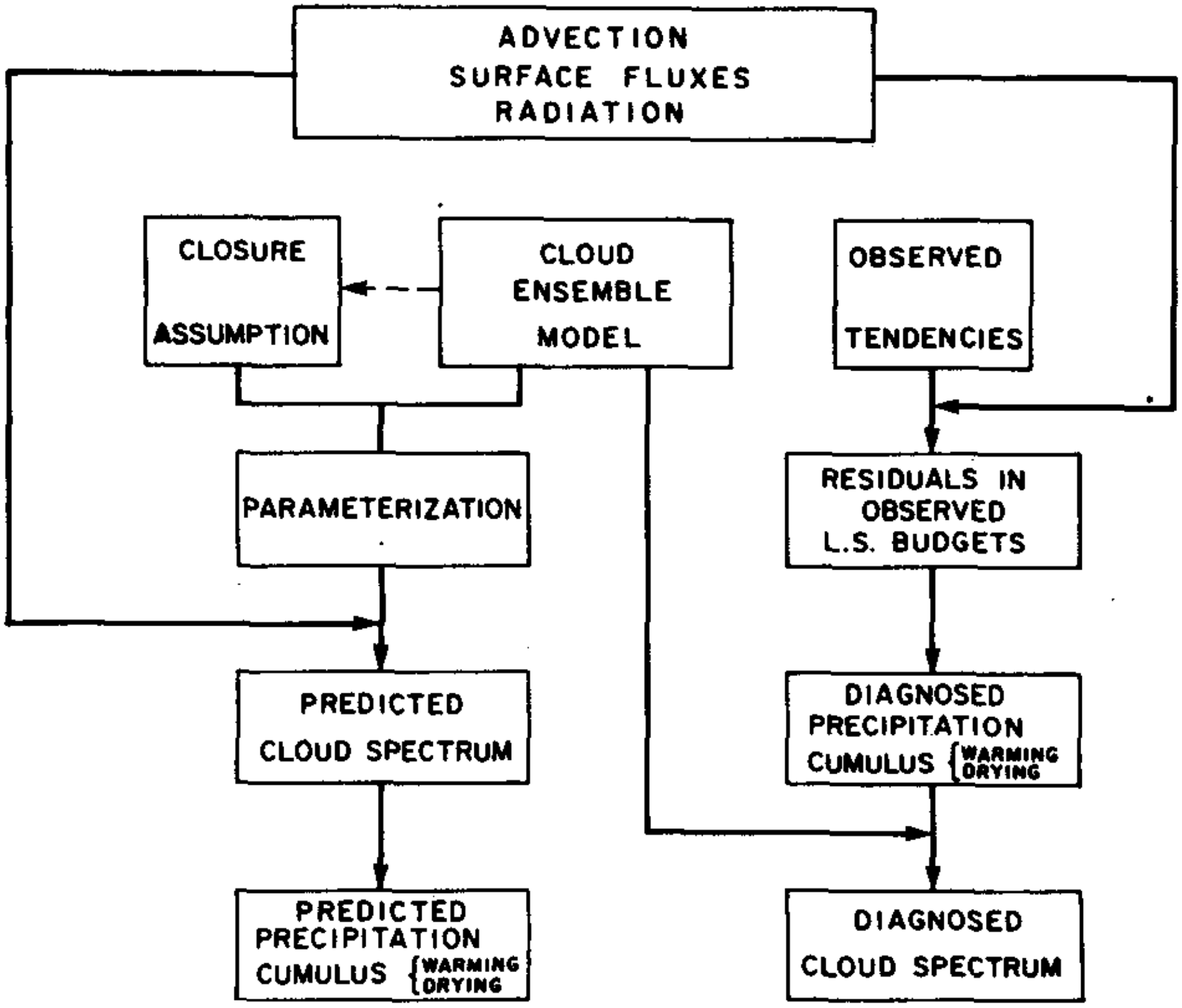

FIG. 1. A schematic diagram showing the role of large-scale observed data in the verification of a cumulus parameterization.

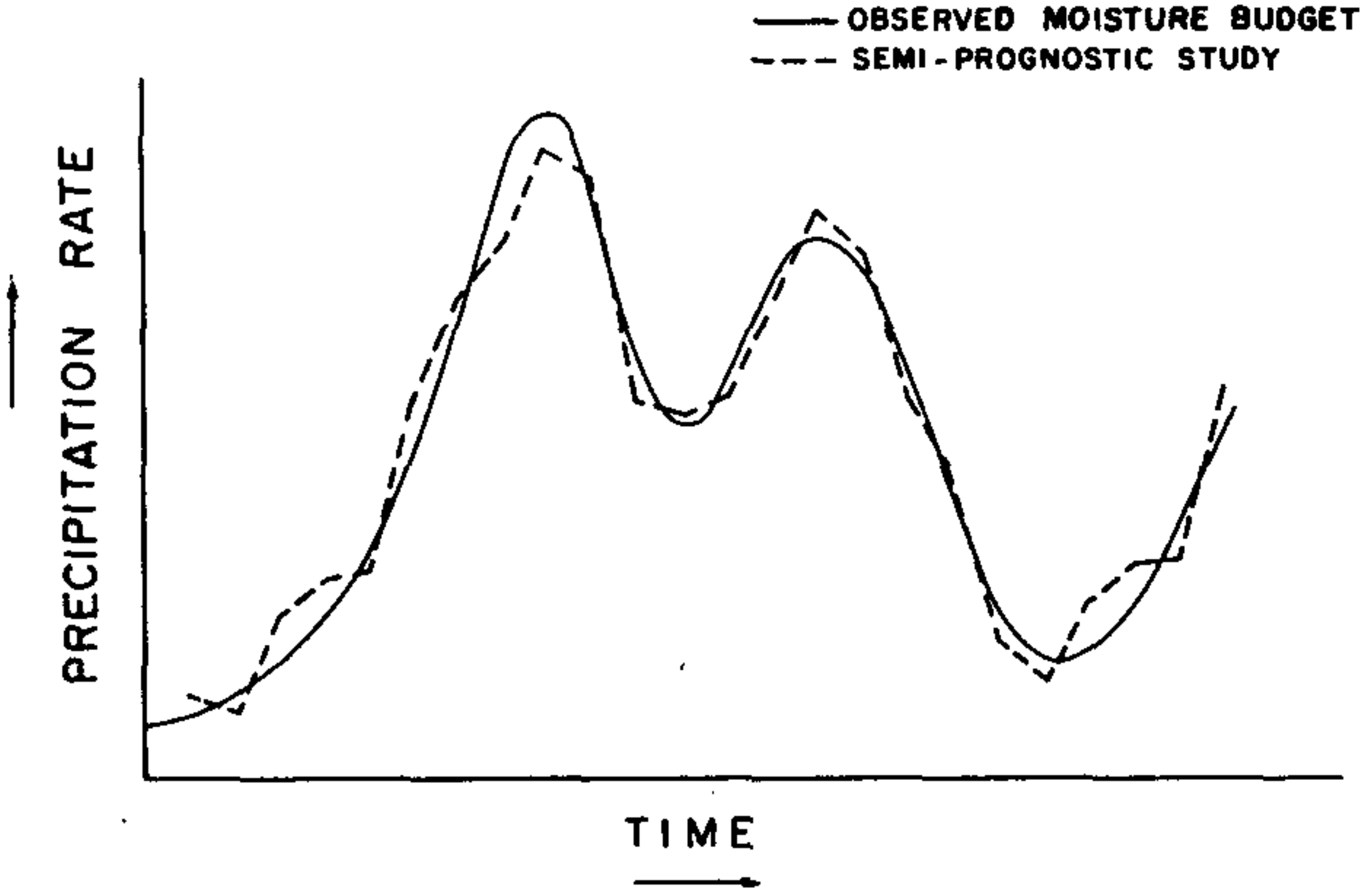

FIG. 2. A schematic diagram comparing the precipitation rates obtained from a semi-prognostic approach and from the observed moisture budget.

Recall that from Parts I and II that the cloud-work function is a generalized measure of the moist convective instability in the large-scale environment and is given in continuous form by

$$A(i) = \int_{z_B}^{\hat{z}(i)} \frac{g}{\bar{T}(z)} \eta(z, i)[T_{vc}(z, i) - \bar{T}_v(z)]dz, \quad (3)$$

The subensemble variables $\eta(z, i)$ and $T_{vc}(z, i)$, and thus $A(i)$, are determined by the vertical distributions of $\bar{T}$ and $\bar{q}_v$, the cloud-base water vapor mixing ratio and moist static energy q_{vm} and h_m, and z_B.

of Cox and Griffith (1978). The large-scale temperature and moisture fields are modified by the advective and radiative processes over a time Δt to give

$$\bar{T}' = \bar{T}_0 + \left[\left(\frac{\partial \bar{T}}{\partial t}\right)_{\text{ADV}} + \left(\frac{\partial \bar{T}}{\partial t}\right)_{\text{RAD}}\right]\Delta t \quad (5a)$$

and

$$\bar{q}'_v = (\bar{q}_v)_0 + \left(\frac{\partial \bar{q}_v}{\partial t}\right)_{\text{ADV}} \Delta t. \quad (5b)$$

Next, the modified fractional entrainment rate $\lambda'(i)$ and cloud-work function $A'(i)$ are calculated from the large-scale fields $\bar{T}'$ and $\bar{q}'_v$. The large-scale forcing for each cloud type is then calculated from

$$F(i) = \frac{A'(i) - A_0(i)}{\Delta t}. \quad (6)$$

The time interval $\Delta t = 30$ min is used in this study.

The large-scale data are taken from the *B*- and *A*/*B*-scale network data for Phase III of GATE as analyzed by Thompson *et al.* (1979). Values of $\bar{T}$, $\bar{q}_v$, their horizontal and vertical derivatives, and all velocity components are given for the center of the *B*-scale array every 3 h at the surface and at 25 mb intervals from 1000 to 100 mb. Details of the analysis procedure are given in Thompson *et al.*

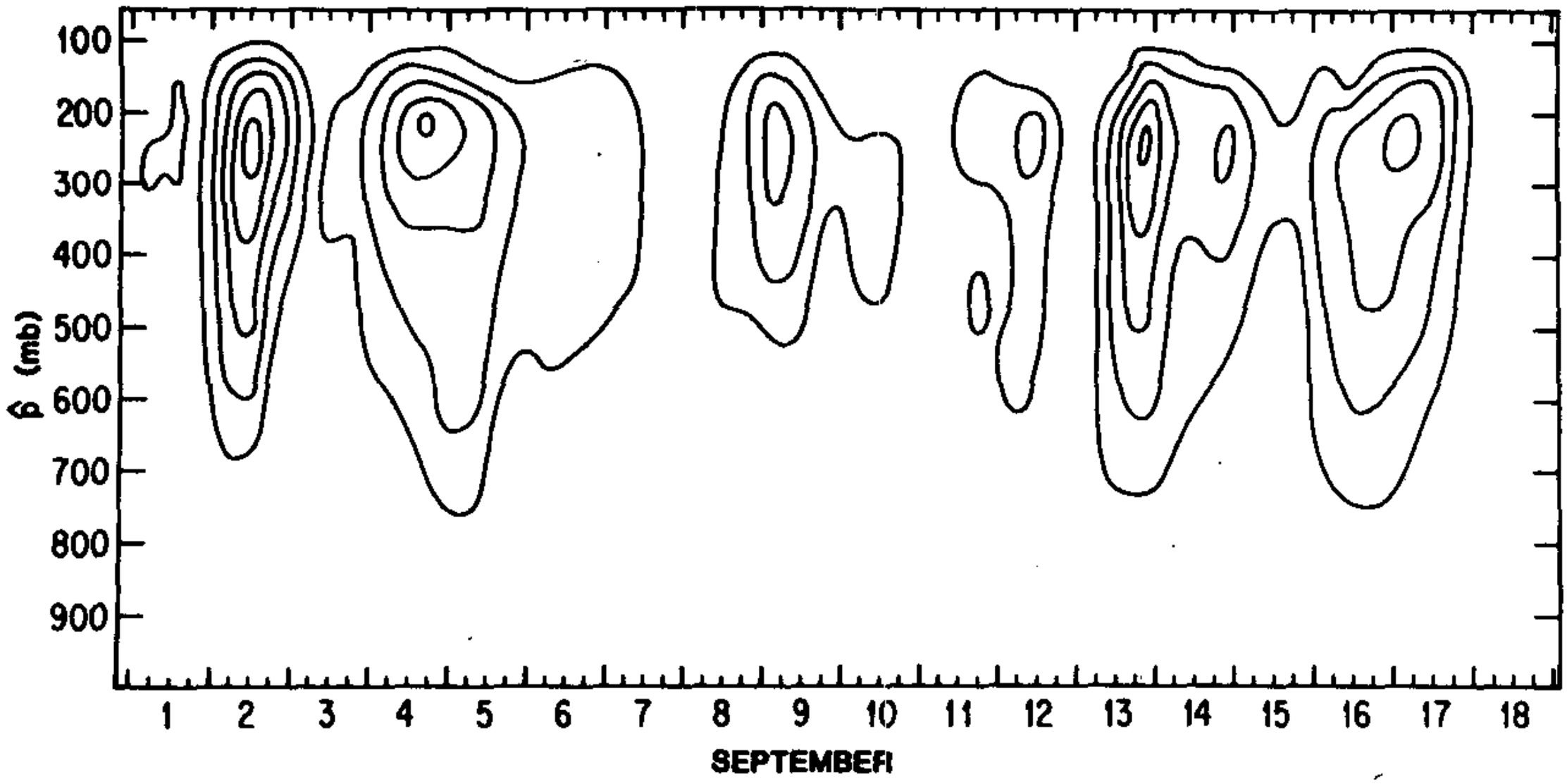

FIG. 4. A time series of the cloud-layer forcing (kJ kg^{-1} day^{-1}) for each cloud type for case Q. The contour interval is 1 kJ kg^{-1} day^{-1}. The ordinate is the cloud-top pressure $\hat{p}$ (mb).

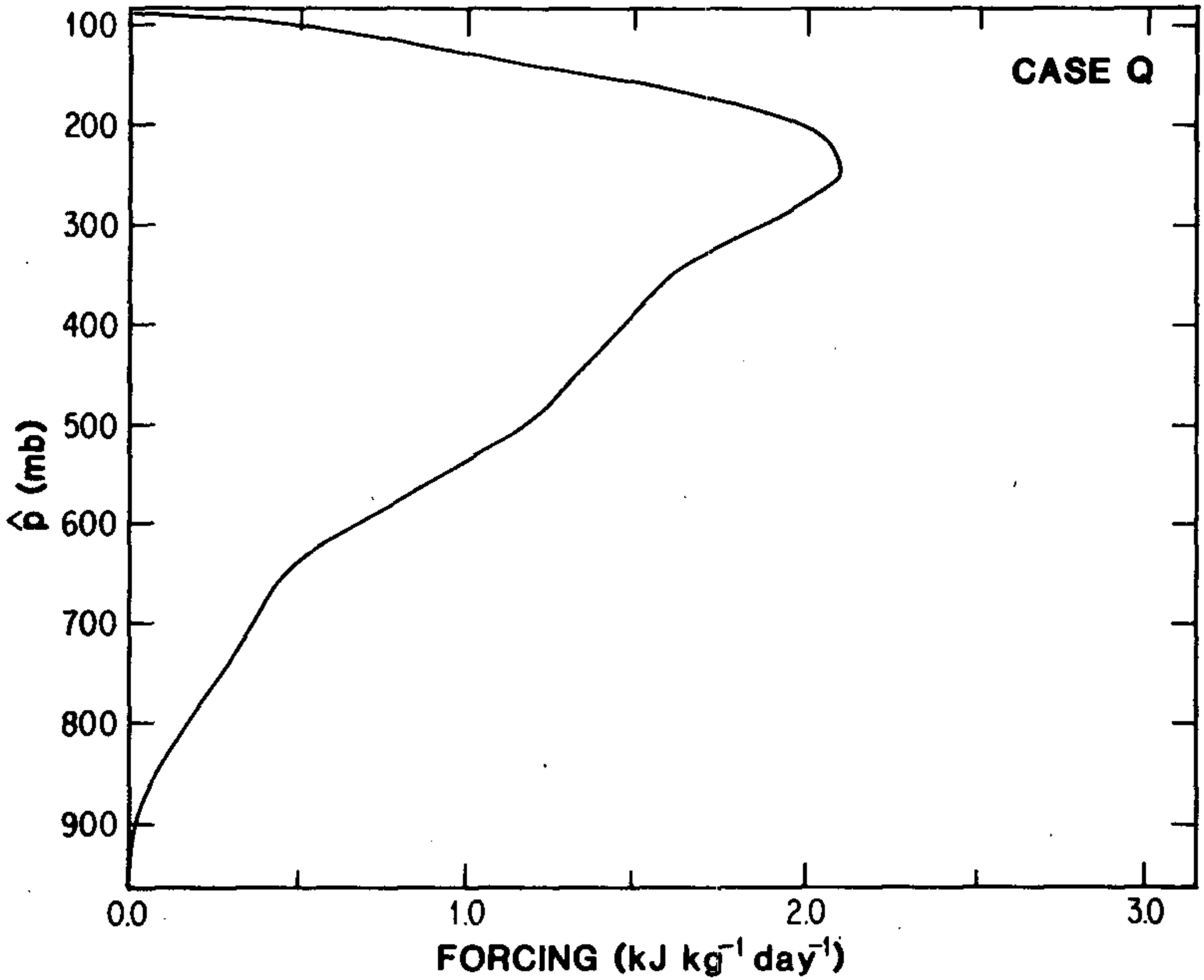

FIG. 5. The time-averaged cloud-layer forcing for case Q over the period 1–18 September. The ordinate is the cloud-top pressure $\hat{p}$ (mb).

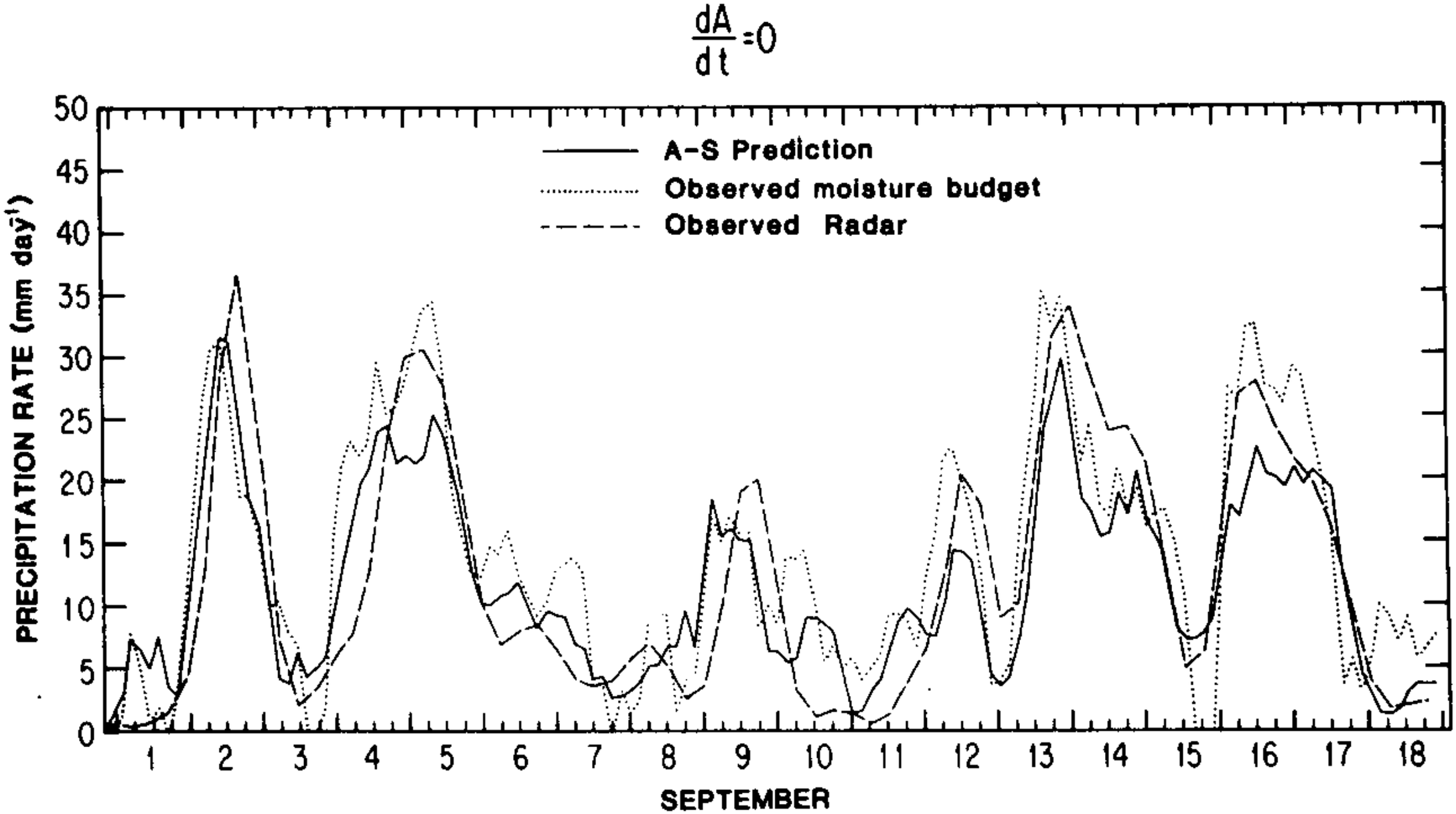

FIG. 6. A time series of precipitation rates (mm day^{-1}) from 1–18 September estimated by case Q, the observed moisture budget and radar.

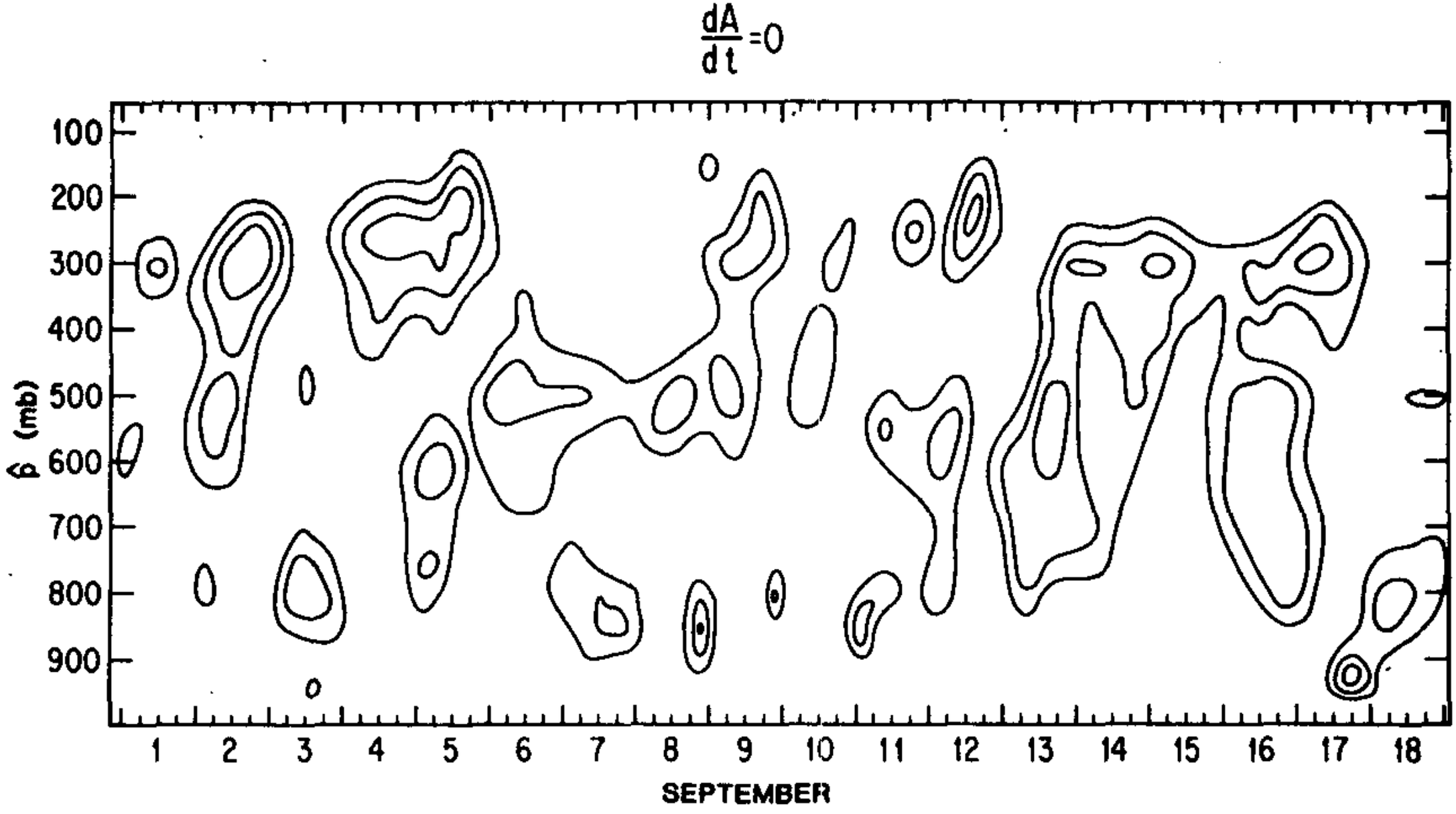

FIG. 7. A time series of cloud-base mass flux (mb h^{-1}) for each cloud type for case *Q*. The contour intervals are 0.25, 0.5, 1.0, 2.0, 4.0 mb h^{-1}.

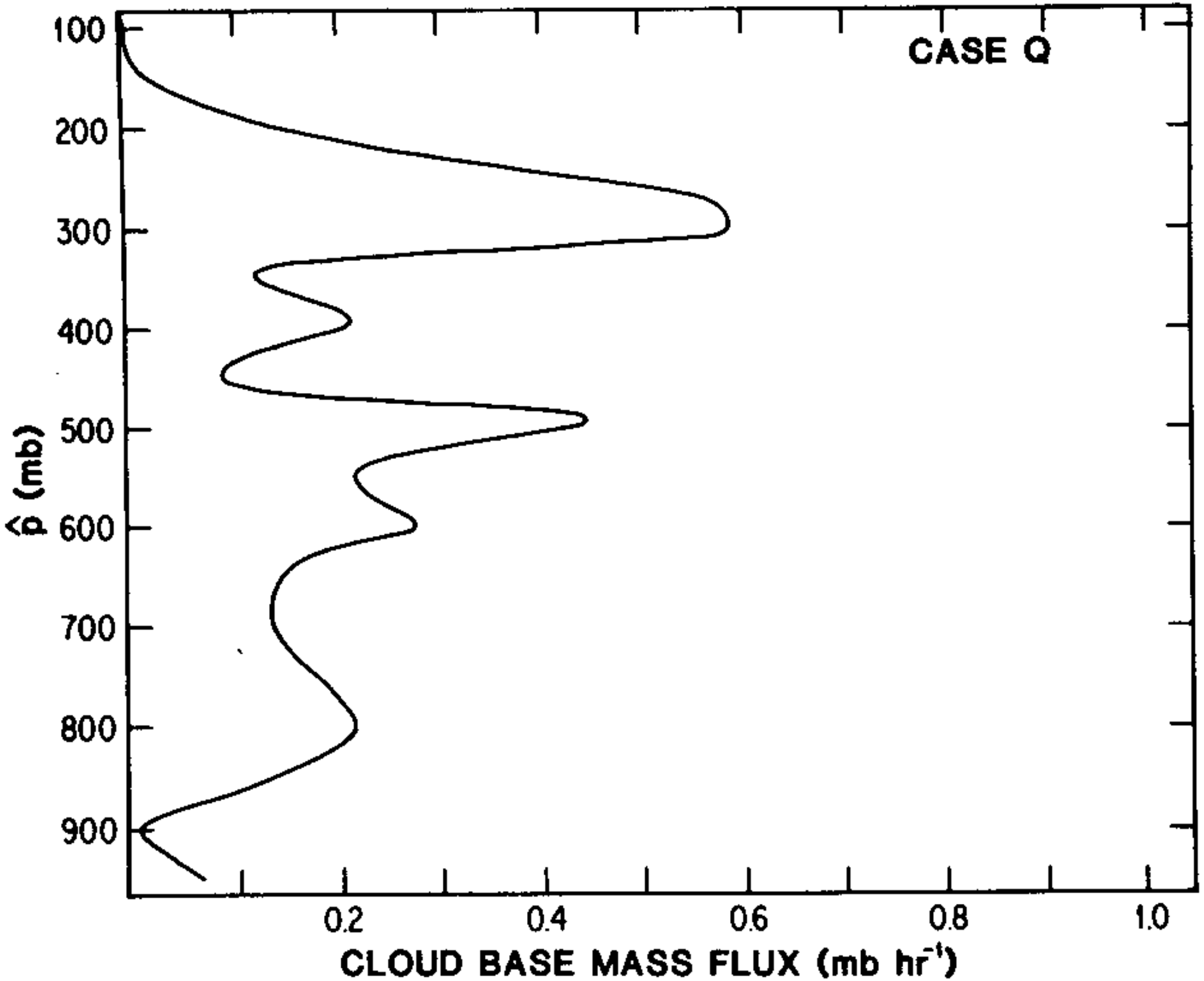

FIG. 8. The time-averaged cloud-base mass flux (mb h^{-1}) for each cloud type for case *Q*.

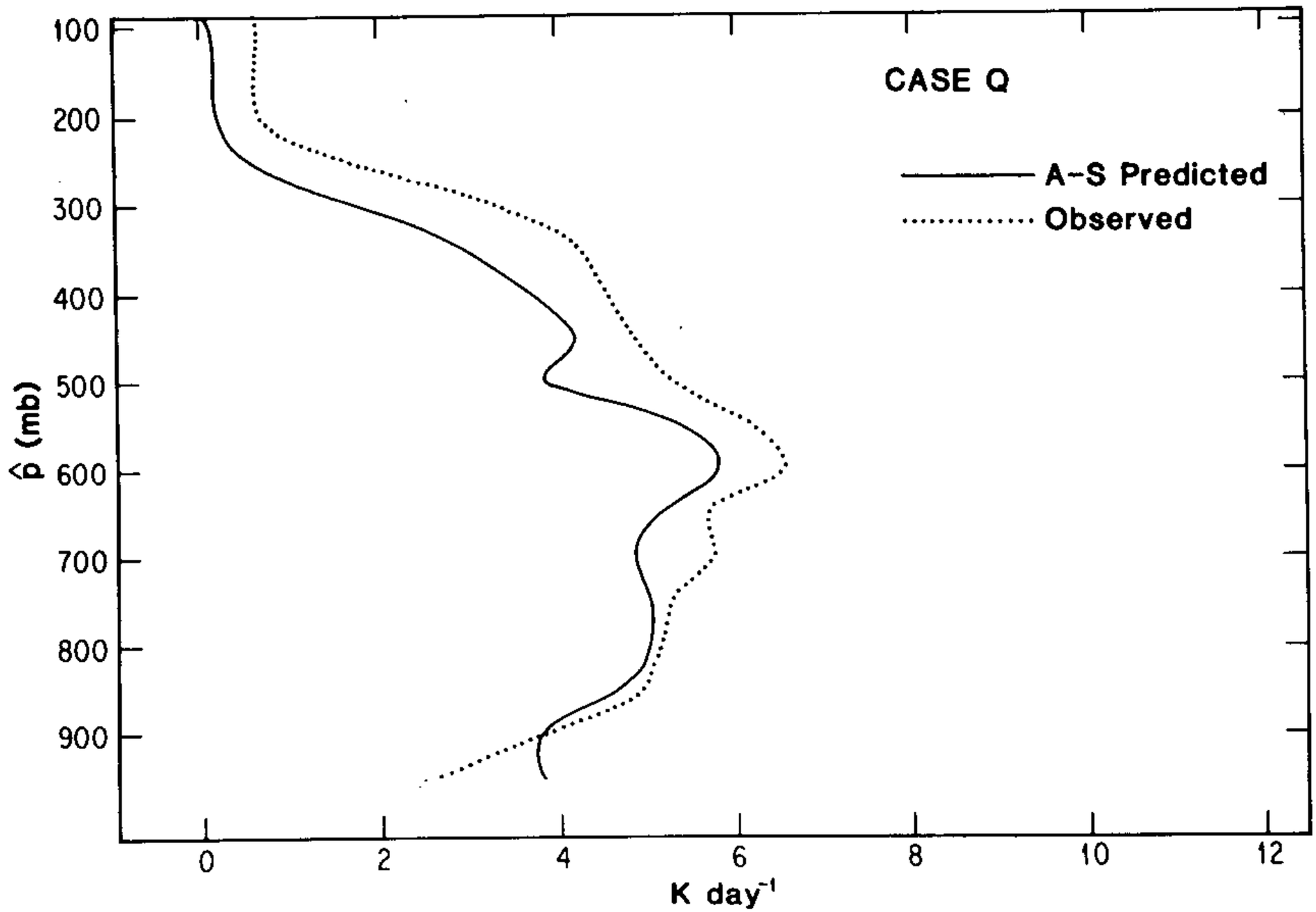

FIG. 9. The time-averaged calculated and observed Q_1–Q_R for case Q.

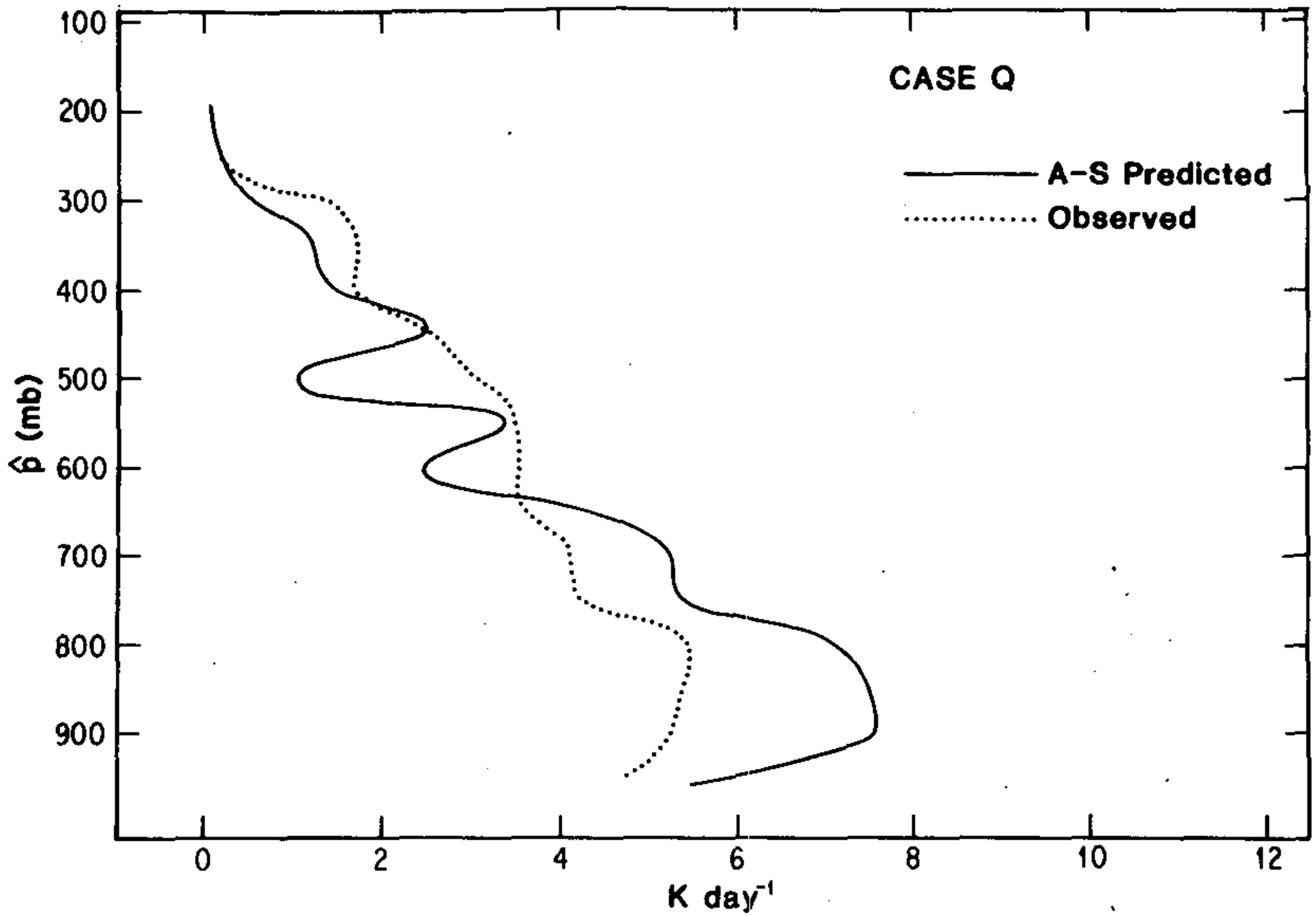

FIG. 10. The time-averaged calculated and observed Q_2 for case Q.

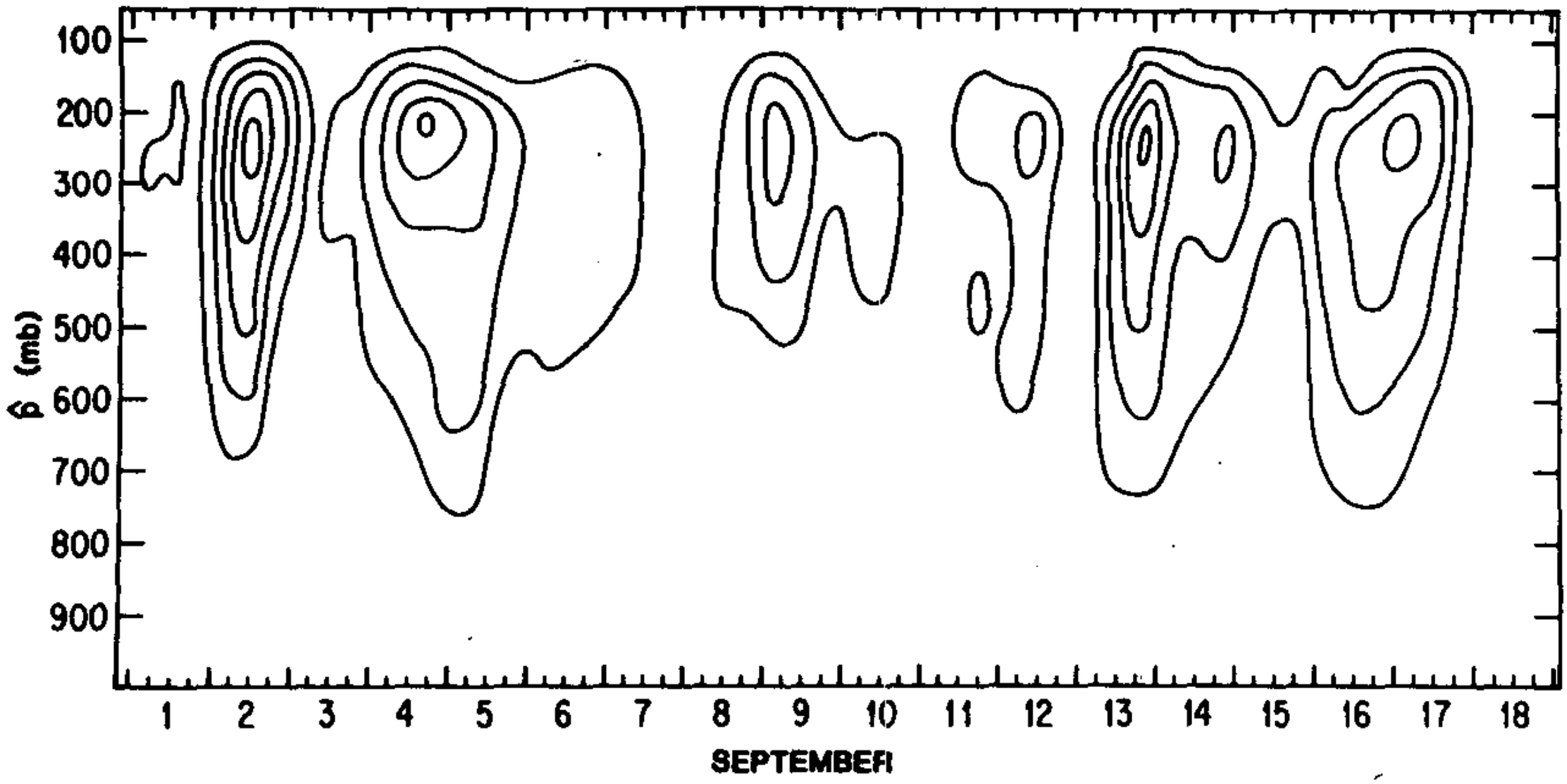

FIG. 4. A time series of the cloud-layer forcing (kJ kg^{-1} day^{-1}) for each cloud type for case Q. The contour interval is 1 kJ kg^{-1} day^{-1}. The ordinate is the cloud-top pressure $\hat{p}$ (mb).

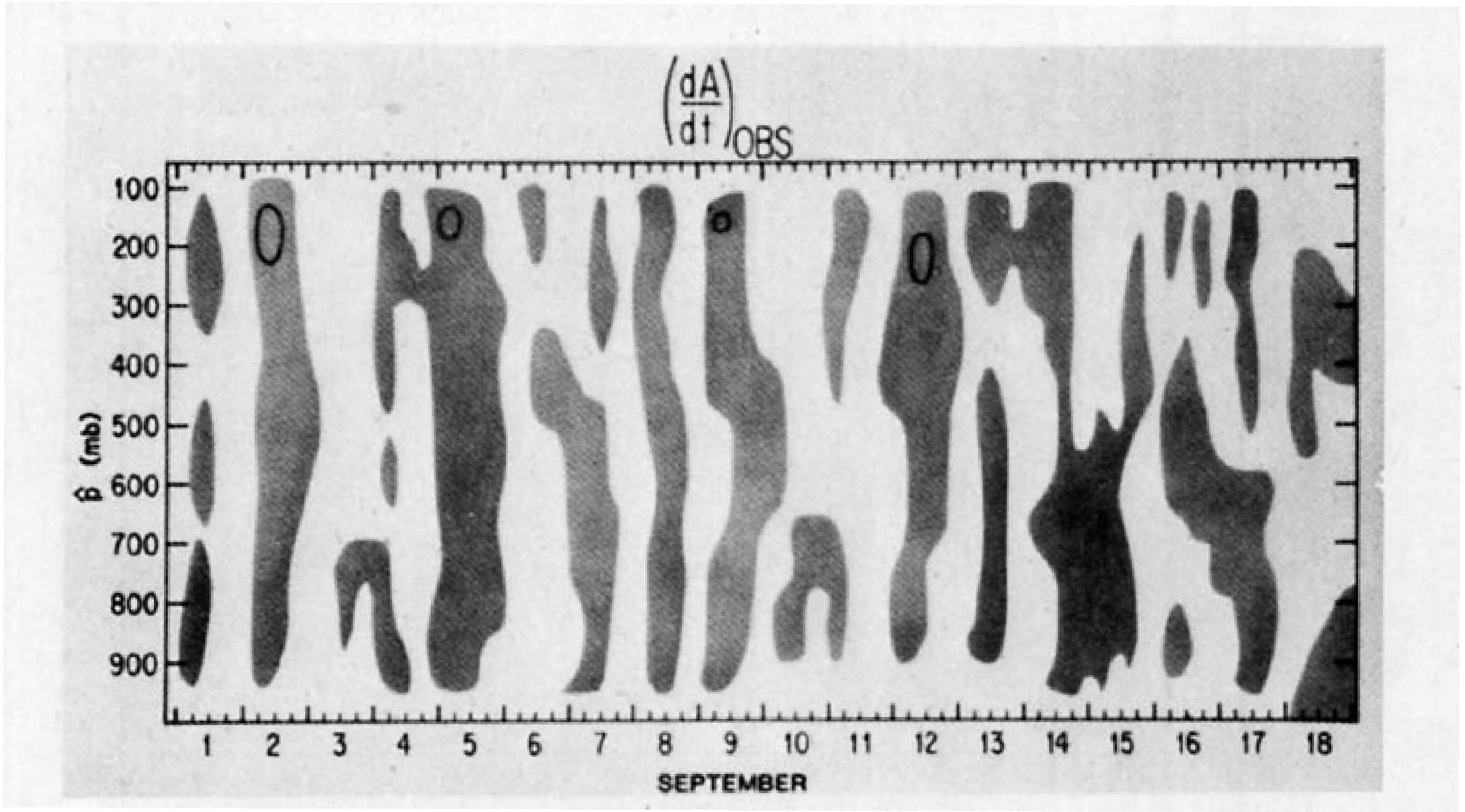

FIG. 11. A time series of $[dA/dt]_{OBS}$ for each cloud type. The contour interval is 1 kJ kg^{-1} day. The shaded area corresponds to $[dA/dt]_{OBS} < 0$.

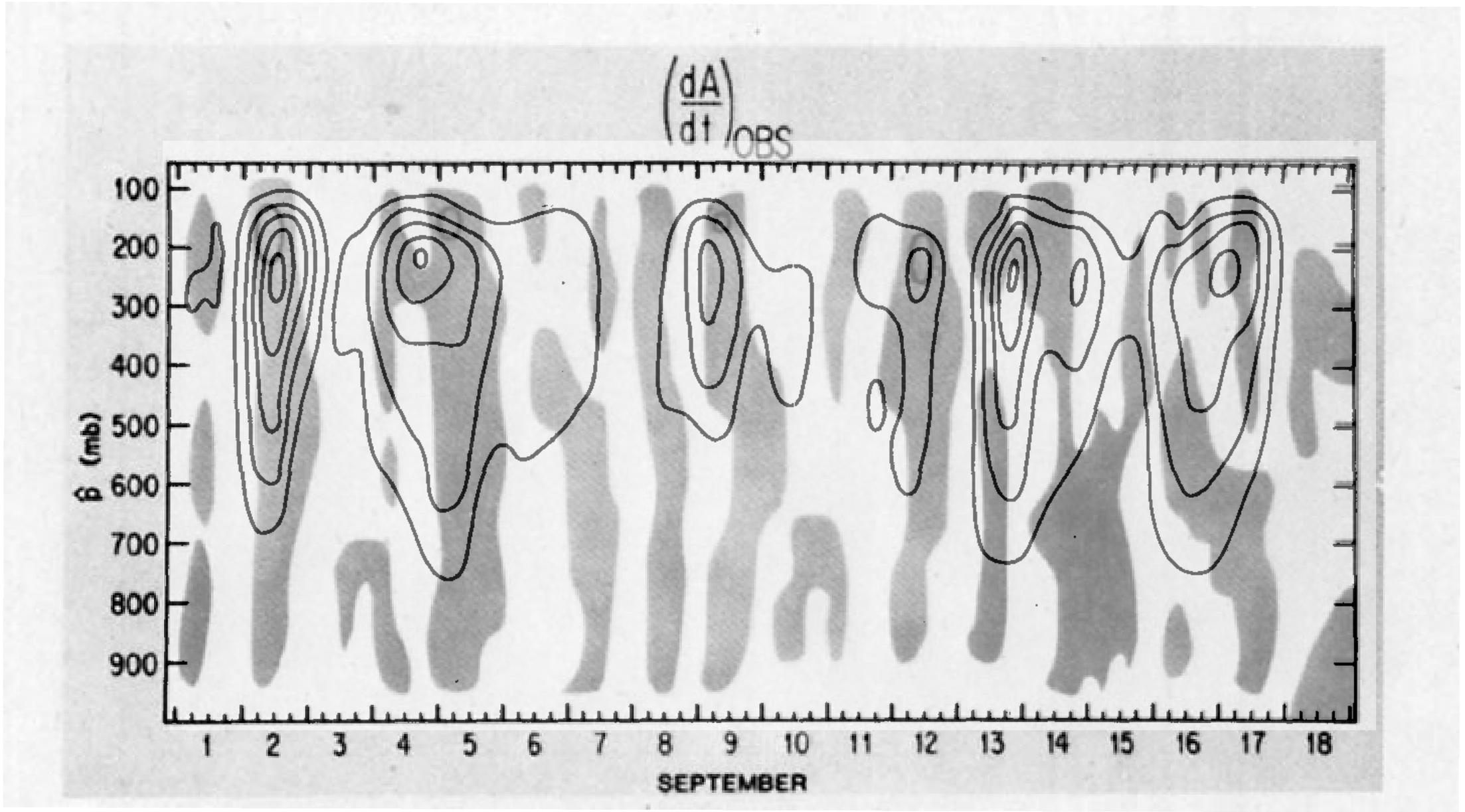

FIG. 11. A time series of $[dA/dt]_{OBS}$ for each cloud type. The contour interval is 1 kJ kg^{-1} day. The shaded area corresponds to $[dA/dt]_{OBS} < 0$.

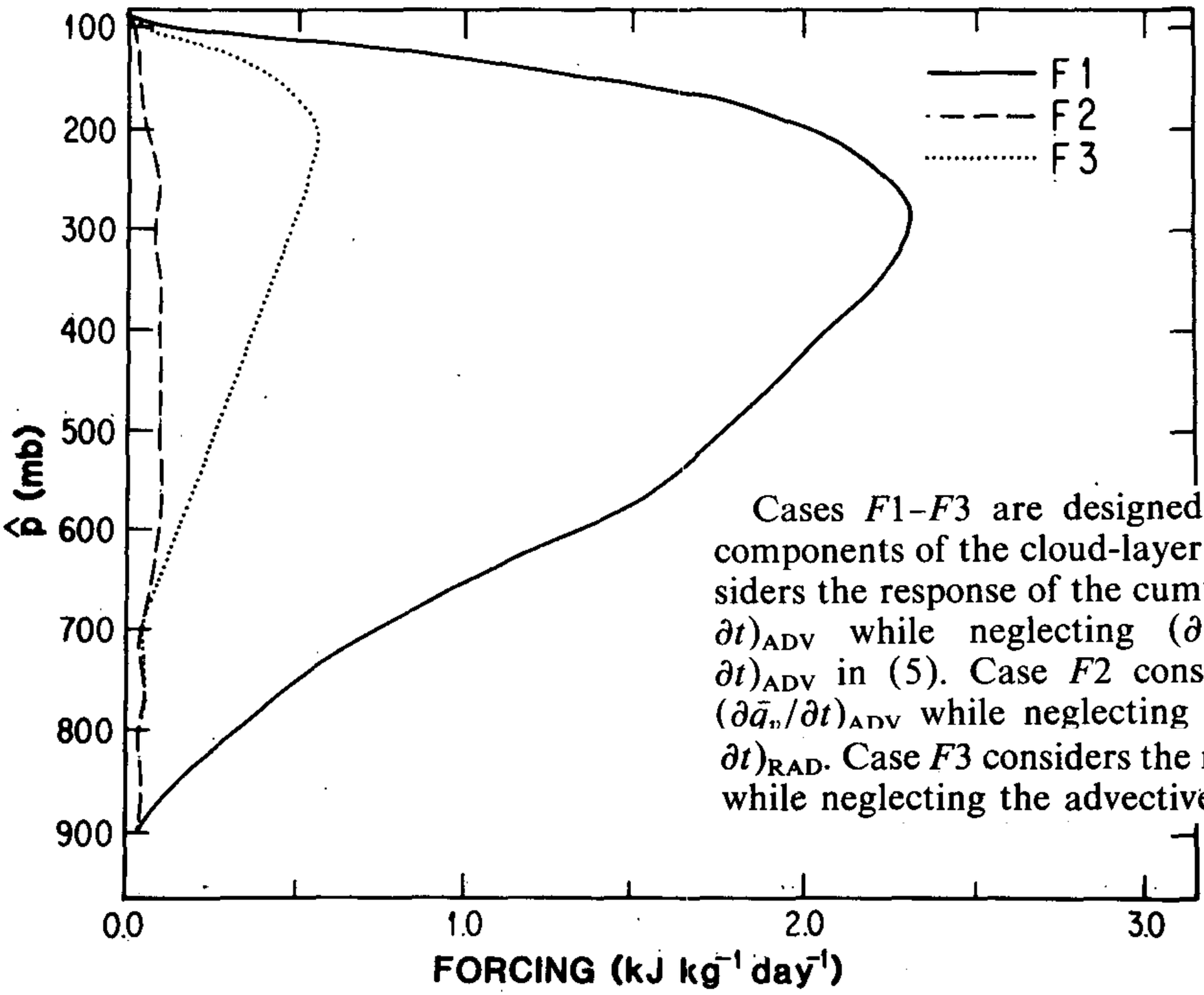

Cases $F1$–$F3$ are designed to show the various components of the cloud-layer forcing. Case $F1$ considers the response of the cumulus ensemble to $(\partial\bar{T}/\partial t)_{\mathrm{ADV}}$ while neglecting $(\partial\bar{T}/\partial t)_{\mathrm{RAD}}$ and $(\partial\bar{q}_v/\partial t)_{\mathrm{ADV}}$ in (5). Case $F2$ considers the response to $(\partial\bar{q}_v/\partial t)_{\mathrm{ADV}}$ while neglecting $(\partial\bar{T}/\partial t)_{\mathrm{ADV}}$ and $(\partial\bar{T}/\partial t)_{\mathrm{RAD}}$. Case $F3$ considers the response to $(\partial\bar{T}/\partial t)_{\mathrm{RAD}}$ while neglecting the advective forcing.

FIG. 14. As in Fig. 5 except for cases $F1$–$F3$.

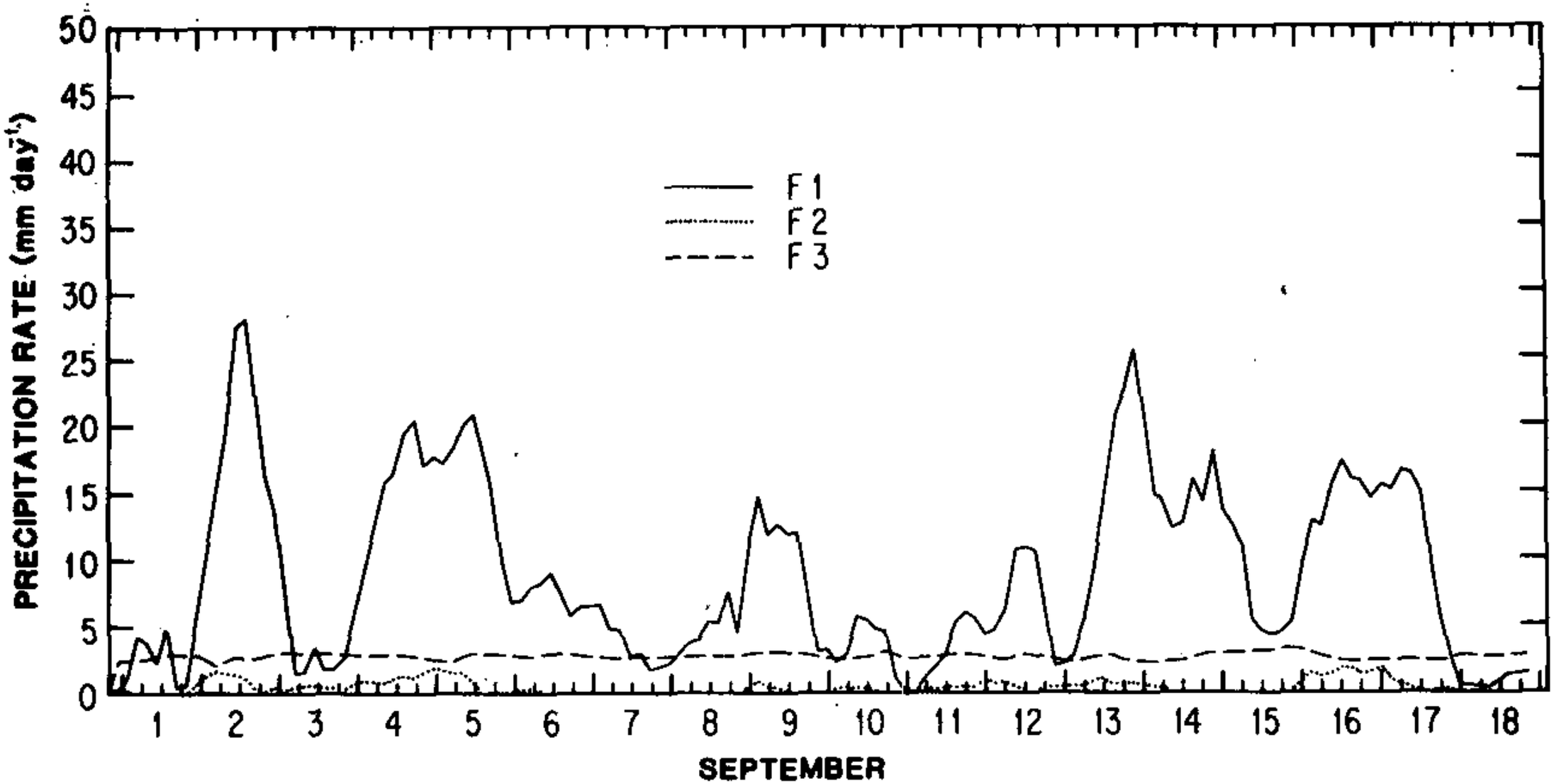

FIG. 15. As in Fig. 6 except for cases *F*1–*F*3.